Pattern Recognition Letters 32 (2011) 2015–2024

Contents lists available at SciVerse ScienceDirect

Pattern Recognition Letters

journal homepage: www.elsevier.com/locate/patrec

Image feature detection from phase congruency based on two-dimensional Hilbert transform ☆

Ke Wang, Pengfeng Xiao *, Xuezhi Feng, Guiping Wu

Department of Geographical Information Science, Nanjing University, No. 22 Hankou Road, Nanjing, Jiangsu 210093, China

ARTICLE INFO

Article history:
Received 5 January 2011
Available online 10 September 2011
Communicated by Y.J. Zhang

Keywords:
Phase congruency
Hilbert transform
Local energy
Feature detection

ABSTRACT

The theory of phase congruency is that features such as step edges, roofs, and deltas always reach the maximum phase of image harmonic components. We propose a modified algorithm of phase congruency to detect image features based on two-dimensional (2-D) discrete Hilbert transform. Windowing technique is introduced to locate image features in the algorithm. Local energy is obtained by convoluting original image with two operators of removing direct current (DC) component over current window and 2-D Hilbert transform, respectively. Then, local energy is divided with the sum of Fourier amplitude of current window to retrieve the value of phase congruency. Meanwhile, we add the DC component of current window on original image to the denominator of phase congruency model to reduce the noise. Finally, the proposed algorithm is compared with some existing algorithm in systematical way. The experimental results of images in Berkeley Segmentation Dataset (BSDS) and remotely sensed images show that this algorithm is readily to detect image features.

1. Introduction

Feature detection is one of the most fundamental tasks in image processing. Image features such as step edges and ramps are the most valuable information that can be extracted for recognition task. Research on the algorithm of feature detection is still insufficient, even though it has been preceded for years.

Most of the pioneering algorithms of feature detection are implemented by convoluting the image with a given operator. There are many famous operators such as those developed by Roberts (1965), Prewitt (1970) and Sobel (1978). Then, Marr and Hildreth (1980) and Canny (1986) introduced more systemic algorithms to retrieve significant edges from images. Except these operators, there are different approaches which have been explored, such as active contour models (Blake, 1998) and level-set method (Sethian, 1996).

In recent years, some new approaches are developed for feature detection, such as wavelet-like filtering (Ducottet et al., 2004; Yi et al., 2009; Zhang and Bao, 2002), neural networks (Lu et al., 2003; Toivanen et al., 2003), rule bases (Bezdek et al., 1998), and fuzzy morphological concepts (De Baets et al., 1994). Even though these recent methods are claimed to have better performance than early ones, application still concern those early and simple methods.

Phase congruency method proposed by Morrone and Owens, (1987) and Morrone and Burr (1988) is an algorithm to detect features according to the phase information, and has been employed into face recognition (Bezalel and Efron, 2005), palm-print verification (Punsawad and Wongsawat, 2009; Struc and Pavesic, 2009), iris recognition (Osman, 2011) and remotely sensed image feature detection (Xiao et al., 2006; Ahmed et al., 2009). Additionally, phase congruency method has been introduced into Image quality assessment (IQA) (Liu and Laganière, 2007; Zhang et al., 2011).

Local energy model was developed by Morrone to detect image features based on one-dimension (1-D) Hilbert transform. We introduce the two-dimensional (2-D) discrete Hilbert transform to simplify the calculation of local energy, and to improve the result of feature detection. We present windowing technique in calculating the local energy, and then normalize the local energy by dividing sum of Fourier amplitude over the current window to point up features in the image. For the existence of noise, direct current (DC) component is introduced into the denominator to reduce noise.

The remainder of the paper is constructed as follows. Section 2 describes the background of previous methods in feature detection and the theory of phase congruency. Section 3 is devoted to construct 2-D local energy model based on 2-D Hilbert transform. Section 4 compares the existing algorithm with the proposed one, and presents experimental results of feature detection on images in Berkeley Segmentation Dataset (BSDS) and remotely sensed images.

☆ This paper is supported by National High Technology Research and Development Program of China (Grant No. 2008AA12Z106) and National Natural Science Foundation of China (Grant No. 40801166).

* Corresponding author. Tel.: +86 25 83593677; fax: +86 25 83592686.
E-mail address: xiaopf@gmail.com (P. Xiao).

0167-8655/$ - see front matter © 2011 Elsevier B.V. All rights reserved.
doi:10.1016/j.patrec.2011.08.013

2. Background

2.1. Gradient-based feature detection methods

Pioneer gradient-based algorithms of feature detection are proposed by Roberts (1965), Prewitt (1970) and Sobel (1978). Then these methods were developed by Marr and Hildreth (1980) based on human perception. They introduced a second derivative operator Laplacian of Gaussian (LoG) with which features can be detected via the zero-crossings of the image. Canny formulated three edge detection criteria: good detection; good localization; and only one response to a single edge (Canny, 1986). Based on these criteria, Canny introduced Gaussian function, which is a low-pass filter, into the gradient-based feature detection method to reduce noise. Subsequently, Deriche (1987) and Shen and Castan (1986) developed two similar operators based on Canny's criteria. These detection operators involve a low-pass filter, such that the better detection result can be retrieved. Koplowitz and Greco (1994) fixed the error of Canny's localization criterion. Additionally, based on these classic operators, Demigny (2002) and Bao et al. (2005) did further researches to improve the performance.

Furthermore, wavelets have been used for multiscale edge analysis. Feature can be detected at the point with the local maxima of the wavelet transform. The edge detection method using wavelet is also relative to the level of intensity gradient. For example, the dyadic wavelet proposed by Mallat and Hwang (1992) is a quadratic spline by approximating the first derivative of Gaussian. The algorithm of wavelets has the same characteristic as classic operators such as Canny and Sobel operator. Namely, when the level of intensity gradient is higher, the detection from the algorithm of wavelet is more distinct.

There are two problems in gradient-based feature detection algorithm. The first problem is that these algorithms are an ideal and single model for step edge. However, there are different kinds of features such as deltas, roofs and ramp profiles. As shown in Fig. 1, Perona and Malik (1990) pointed out that image features are more a combination of steps, deltas, roofs and ramp profiles. In the general situation, features will be far more complex than Fig. 1. Thus, it is difficult to detect image features using gradient-based operator readily. The second problem is that it is easy to be influenced by the level of intensity gradient in the image. In the post-processing thresholding, edges with low level of intensity gradient may be ignored. Thus, good detection cannot be obtained before cognizing the level of contrast or the magnification of the image. Additionally, other edge detection approaches are also susceptible to gradient information, such as active contours model.

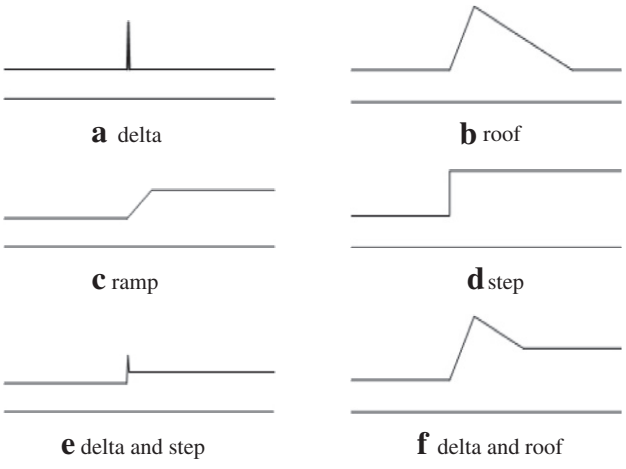

Fig. 1. Different types of image features. (a), (b), (c), and (d) show cases of delta, roof, ramp, and step; (e) and (f) show the simple situation of feature with a combination of delta and step, delta and roof.

2.2. Review of phase congruency

In the research on the phenomenon of Mach band, Morrone et al. (1986) found that there is a high phase congruency where feature can be perceived in the image. A signal can be expressed as the sum of different harmonic components using Fourier transform. Fig. 2 is a one-dimension signal with step, eight harmonic components of this signal and the sum of these harmonic components. It shows that all eight harmonic components share the same phase (the phase is zero) at the point of step. Furthermore, the principle is the same with the feature like delta, roof and ramp.

Based on the theory of phase congruency, local energy is introduced to detect features. Morrone and Burr (1988) and Morrone and Owens (1987) calculated the local energy using the original signal and its 1-D Hilbert transform, but it is not convenient that local energy is calculated by horizontal and vertical orientation, respectively. Subsequently, Kovesi (1999, 2000) developed a novel algorithm to calculate the local energy by using the odd and even log Gabor wavelet. Two variant of ε and T are introduced into this algorithm to reduce noise. T is decided by the situation of noise in the image, thus, it will involve more complex calculation. Additionally, ε can influence the detection result, and it should be more reasonable.

Morrone et al. (1986) showed the fundamental principle of phase congruency was that image features which can be perceived always relate to points with strong phase congruency in the image. For example, let $f(x) \in L^2(T)$, and the signal of $F(x)$ can be developed into Fourier series expansion which is defined by

$$f(x) = \sum_n a_n \sin(nx + \phi_{n_0}) = \sum_n a_n \sin(\phi_n(x)) \quad n \geqslant 0,\ a_n > 0, \tag{1}$$

where a_n, x and ϕ_n are the amplitude, angular frequency and initial phase of nth-degree harmonic, respectively.

When $\phi_n(x_i) = 90°$, $f(x_i)$ comes to $\sum_n a_n$, which is the sum of Fourier amplitude. For $\phi_n(x_i) = 0°$, $f(x_i)$ comes to zero. If every $\phi_n(x_i)$ of the point is the same but not 90° or 0°, the feature cannot be extracted easily. Thus, Morrone introduced Hilbert transform to determine the feature point with strong phase congruency. After Hilbert transform, the Fourier series expansion of signal has the same amplitude spectrum, and phases of negative and positive frequency component have a 90° and a −90° offset, respectively. Thus, according to Eq. (1), the Hilbert transform $\hat{f}(x)$ of $f(x)$ can be given by

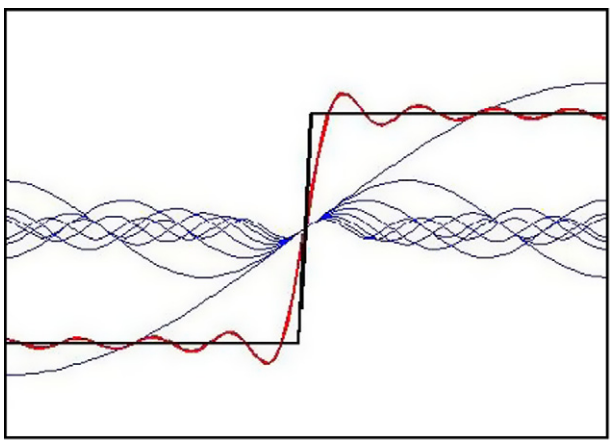

Fig. 2. Fourier series of a step feature and the sum of eight harmonic components.

$$\hat{f}(x) = \sum_n a_n \cos(nx + \phi_{n_0}) = \sum_n a_n \cos(\phi_n(x)) \quad n > 0. \tag{2}$$

According to Parseval's theorem, the relation of the norm of $\hat{f}(x)$ of $f(x)$ can be present by

$$\|\hat{f}(x)\|_2^2 = \|f(x)\|_2^2 - |a_0|^2, \tag{3}$$

where a_0 is the first harmonic component of Fourier transform of the signal $f(x)$.

According to Parseval's theorem and the fact that Hilbert transform is skew-symmetric, a proposition (Eq. (4)) can be proved

$$\int f(x)\hat{f}(x)dx = 0. \tag{4}$$

Because $\hat{f}(x)$ of $f(x)$ is quadrature pair, a function of local energy $E(x)$ can be defined by

$$E(x) = \sqrt{f^2(x) + \hat{f}^2(x)}. \tag{5}$$

Considering Eq. (1), (2), and (5), the local energy can be spread as

$$E(x) = \sqrt{\left(\sum_n a_n \sin(\phi_n(x))\right)^2 + \left(\sum_n a_n \cos(\phi_n(x))\right)^2}. \tag{6}$$

When the phase congruency happens to one point of the signal, the phase of every harmonic of the point is the same value $\phi(x)$.Thus, Eq. (6) can be delivered as

$$\begin{aligned} E(x) &= \sqrt{\sin(\phi(x))^2\left(\sum_n a_n\right)^2 + \cos(\phi(x))^2\left(\sum_n a_n\right)^2} \\ &= \sum_n a_n \sqrt{\sin(\phi(x))^2 + \cos(\phi(x))^2} = \sum_n a_n. \end{aligned} \tag{7}$$

The maximum of local energy is no larger than the sum of amplitude spectrum ($\sum_n a_n$), such that it can be normalized by $\sum_n a_n$ to define phase congruency

$$PC(x) = \frac{E(x)}{\sum_n a_n}. \tag{8}$$

Thus, the value of PC is the result of local energy normalized by the sum of Fourier amplitude. Meanwhile, the normalization of local energy can make features detection more legible.

3. 2-D phase congruency model

In this section, we introduce 2-D Hilbert transform into calculation of PC to make the detection more convenient and accurate. Meanwhile, the necessity of removing DC component in the calculation of local energy and windowing is discussed. Then, we introduce two operators of 2-D Hilbert transform and removing DC component to simplify the calculation of local energy. Finally, we introduce the DC component of current window over original image into the algorithm to reduce the noise.

3.1. 1-D discrete Hilbert transform

1-D discrete Hilbert transform (DHT) is present in frequency and spatial domain, before introducing the 2-D discrete Hilbert transform. Let $f(x)$ is discrete signal, $\hat{f}(x)$ can be obtained by

$$\hat{f}(x) = f(x) * h(x), \tag{9a}$$

where

$$h(x) = \frac{1 - (-1)^x}{x\pi} \quad x = 1, 2, 3 \ldots \tag{9b}$$

Using the Fourier transform, $\hat{f}(x)$ also can be obtained by

$$\begin{aligned} \hat{f}(x) &= IDFT[\widehat{F}(j\Omega)] = IDFT[F(j\Omega)H(j\Omega)] \\ &= IDFT[F(j\Omega)[-jsgn(\Omega)]], \end{aligned} \tag{10}$$

where $\widehat{F}(j\Omega)$ and $F(j\Omega)$ is the Fourier transform of $\hat{f}(x)$ and $f(x)$, respectively; $IDFT$ is Inverse Discrete Fourier transform; Ω is the angular frequency. And the function $H(j\Omega)$ can be delivered as

$$H(j\Omega) = -jsgn(\Omega) = \begin{cases} -j & \Omega > 0, \\ j & \Omega < 0, \end{cases} \tag{11}$$

where Ω is angular frequency; $sgn(\Omega)$ denotes the finite discrete signum function.

According to Eq. (11), the frequency of DC component which is the first harmonic component a_0 of the signal, is zero, thus, the DC component of the signal is removed after Hilbert transform. This is equivalent to saying that the mean of the signal is zero after Hilbert transform, because of the fact that DC component is relative with the mean of the signal.

3.2. 2-D discrete Hilbert transform

Based on 1-D discrete Hilbert transform, it is complicated to compute the local energy by horizontal and vertical orientation, respectively. We introduce 2-D discrete Hilbert transform into the construction of local energy, such that image features can be detected readily. For 2-D Hilbert transform, there are several forms such as Riesz transform (Felsberg and Sommer, 2001) which is also used in signal processing like IQA (Zhang et al., 2010). The 2-D Discrete Hilbert Transform used in this paper is defined by Read and Treitel (1973) in both the frequency and spatial domain. Given that the odd and even parts of 2-D casual pulse in frequency domain are denoted by $P_e(i,j)$ and $P_o(i,j)$, respectively, an equation related with 2-D DHT can be expressed by

$$P_o(i,j) = [sgn(i,j) + bdy(i,j)]P_e(i,j), \tag{12a}$$

$$sgn(i,j) = \begin{cases} 1 & 0 < i < \frac{N_1}{2}, 0 < j < \frac{N_2}{2}, \\ -1 & \frac{N_1}{2} < i < N_1, \frac{N_2}{2} < j < N_2, \\ 0 & elsewhere, \end{cases} \tag{12b}$$

$$bdy(i,j) = \begin{cases} 1 & j = 0, 0 < i < \frac{N_1}{2}, \\ -1 & j = 0, \frac{N_1}{2} < i < N_1, \\ 1 & i = 0, 0 < j < \frac{N_2}{2}, , \\ -1 & i = 0, \frac{N_2}{2} < j < N_2 \\ 0 & elsewhere, \end{cases} \tag{12c}$$

where $sgn(i,j)$ denotes the finite discrete signum function, and $bdy(i,j)$ is used to adjust the boundary. N_1 and N_2 are the size of $P_e(i,j)$ and $P_o(i,j)$. Given a 2-D signal $X(i,j)$ in frequency domain, the 2-D DHT $\widehat{X}(i,j)$ can be defined by

$$\widehat{X}(i,j) = [sgn(i,j) + bdy(i,j)] \cdot X(i,j), \tag{13}$$

where $i = 0, 1, 2, \ldots, N_1 - 1$, and $j = 0, 1, 2, \ldots, N_2 - 1$.

Let $f(x,y)$ be the 2-D signal in spatial domain, the 2-D DHT of $f(x,y)$ can be retrieved by

$$\hat{f}(x,y) = f(x,y) * h(x,y), \tag{14a}$$

$$h(x,y) = \left(\cot\left(\frac{\pi}{N_1}\right)x + \cot\left(\frac{\pi}{N_2}\right)y\right)\frac{2}{N_1 N_2}, \tag{14b}$$

where $x = 0, 1, 2, \ldots, N_1 - 1$, and $y = 0, 1, 2, \ldots, N_2 - 1$; N_1 and N_2 are the size of image.

Zetzsche and Barth (1990) classified signals into three elementary categories: (1) constant signals that show no variation at all; (2) intrinsically 1-D signals that are constant along one orientation and can, therefore, be completely characterized by their variation along the orthogonal orientation (here: 1-D signals); (3) actually 2-D signals that vary along all orientations (here: 2-D signals). The requirement of detectors for 2-D signals is that they should not respond to 1-D signal erroneously.

The 2-D phase congruency model proposed in this paper, have no error response to 1-D signals, because of the same mathematic principle between 1-D and 2-D Hilbert transform. The image $f(x,y)$ can be expanded as 2-D Fourier series

$$f(x,y) = \frac{1}{MN}\sum_{u=0}^{M-1}\sum_{v=0}^{N-1}|F(u,v)|\sin(\phi_{u,v}(x,y)), \tag{15}$$

where $F(u,v) = \sum_{x=0}^{M-1}\sum_{y=0}^{N-1} f(x,y)e^{-j2\pi(\frac{ux}{M}+\frac{vy}{N})}$; $u = 0,1,2,\ldots,M-1$, and $y = 0,1,2,\ldots,N-1$; M and N are the size of image.

Considering Eq. (5), the local energy $E(x,y)$ can be expressed as

$$E(x,y) = \sqrt{\left(\frac{1}{MN}\sum_{u=0}^{M-1}\sum_{v=0}^{N-1}|F(u,v)|\sin(\phi_{u,v}(x,y))\right)^2 + \left(\frac{1}{MN}\sum_{u=0}^{M-1}\sum_{v=0}^{N-1}|F(u,v)|\cos(\phi_{u,v}(x,y))\right)^2}. \tag{16}$$

When phase congruency happens at the point $f(x,y)$, every phase of $\phi_{u,v}(x,y)$ at point (x,y) has the same value. Thus, Eq. (16) can be delivered as

$$\begin{aligned} E(x,y) &= \frac{1}{MN}\sum_{u=0}^{M-1}\sum_{v=0}^{N-1}|F(u,v)|\sqrt{(\sin(\phi_{u,v}(x,y)) + \cos(\phi_{u,v}(x,y)))^2} \\ &= \frac{1}{MN}\sum_{u=0}^{M-1}\sum_{v=0}^{N-1}|F(u,v)|. \end{aligned} \tag{17}$$

Thus, according to Eq. (8), the phase congruency based on 2-D Hilbert transform can be defined as

$$PC(x,y) = \frac{E(x,y)}{\frac{1}{MN}\sum_{u=0}^{M-1}\sum_{v=0}^{N-1}|F(u,v)|}. \tag{18}$$

In the image processing, step, line and corner are important 2-D image features. Fig. 3 gives three image features to verify the viability of phase congruency model based on 2-D discrete Hilbert transform to detect 2-D image features.

In Fig. 3, the detection result of Fig. 3d and e shows that image features like corner (Fig. 3a) and step (Fig. 3b) can be detected distinctly by using the algorithm proposed in this paper, meanwhile the response of left line in Fig. 3c is also distinct. Additionally, as shown in the detection result of Fig. 3f, the proposed algorithm response the 1-D signal feature (the right line in Fig. 3c) correctly.

3.3. Implementation

Morrone et al. (1986) proved that when the mean of $f(x,y)$ is zero, the maximum of local energy can uniquely determine image features. $\hat{f}(x,y)$ obtained by Hilbert transform always has zero mean value, thus the mean of $f(x,y)$ should be zero to make the maximum of local energy function which is also a zero-crossing of $f(x,y)$ and a peak of $\hat{f}(x,y)$, to uniquely determine a feature. The mean of $f(x,y)$ is relative to the DC component, thus the mean of $f(x,y)$ can be set to zero by removing the DC component. Some experimental results (Fig. 4) are present to prove the necessity of removing DC component for the local energy. As shown in Fig. 4a, feature points of the signal locate at 20, 180, and 360. In Fig. 4b, without removing the DC component of the signal, local energy of three points are 2.3452, 3.5718 and 4.6117, respectively. Because the local energy of points between 180 and 360 is higher than the point at 20, it is difficult to distinguish the feature point at 20 from points between 180 and 360. After removing the DC component of the signal (Fig. 4c), the distribution of maximum of local energy is more centralized and closer as shown in Fig. 4d, and it is more effortless to determine feature points.

Thus, we introduce an operator to remove the DC component, which is convenient to make the mean of the current window be zero in the convolution. The expression is illustrated by

$$\boldsymbol{M} = \begin{bmatrix} -\frac{1}{N\times N} & -\frac{1}{N\times N} & \cdots & -\frac{1}{N\times N} & -\frac{1}{N\times N} \\ -\frac{1}{N\times N} & -\frac{1}{N\times N} & \cdots & -\frac{1}{N\times N} & -\frac{1}{N\times N} \\ \vdots & \vdots & 1-\frac{1}{N\times N} & \vdots & \vdots \\ -\frac{1}{N\times N} & -\frac{1}{N\times N} & \cdots & -\frac{1}{N\times N} & -\frac{1}{N\times N} \\ -\frac{1}{N\times N} & -\frac{1}{N\times N} & \cdots & -\frac{1}{N\times N} & -\frac{1}{N\times N} \end{bmatrix}, \tag{19}$$

where N is the size of matrix $\boldsymbol{M}$.

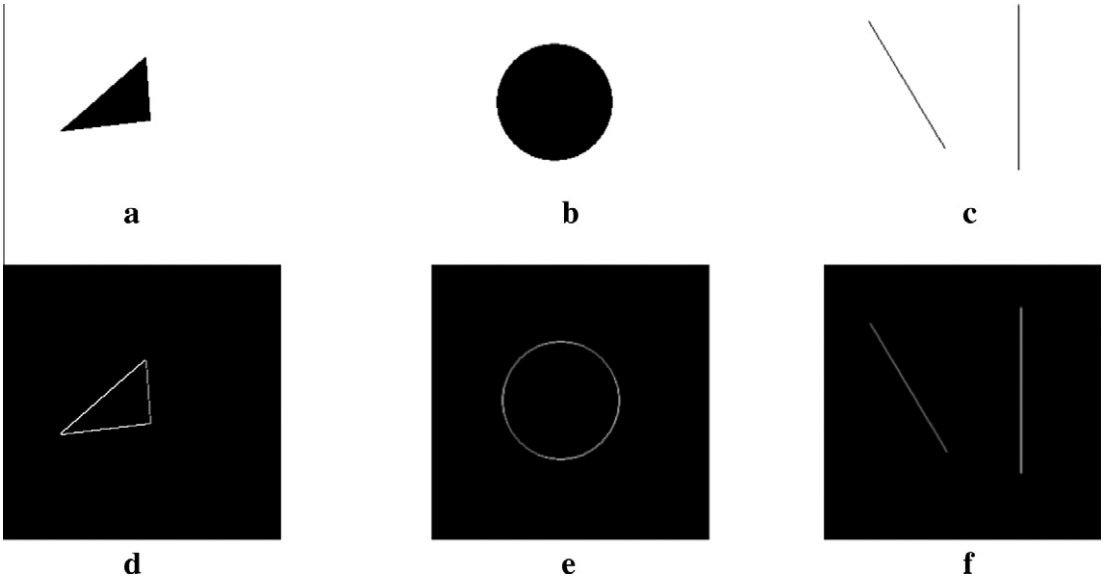

Fig. 3. Different types of 2-D image features. (a) and (b) show cases of step and corner; (c) shows two line features, the left one present 2-D line feature and the right one present 1-D signal feature.

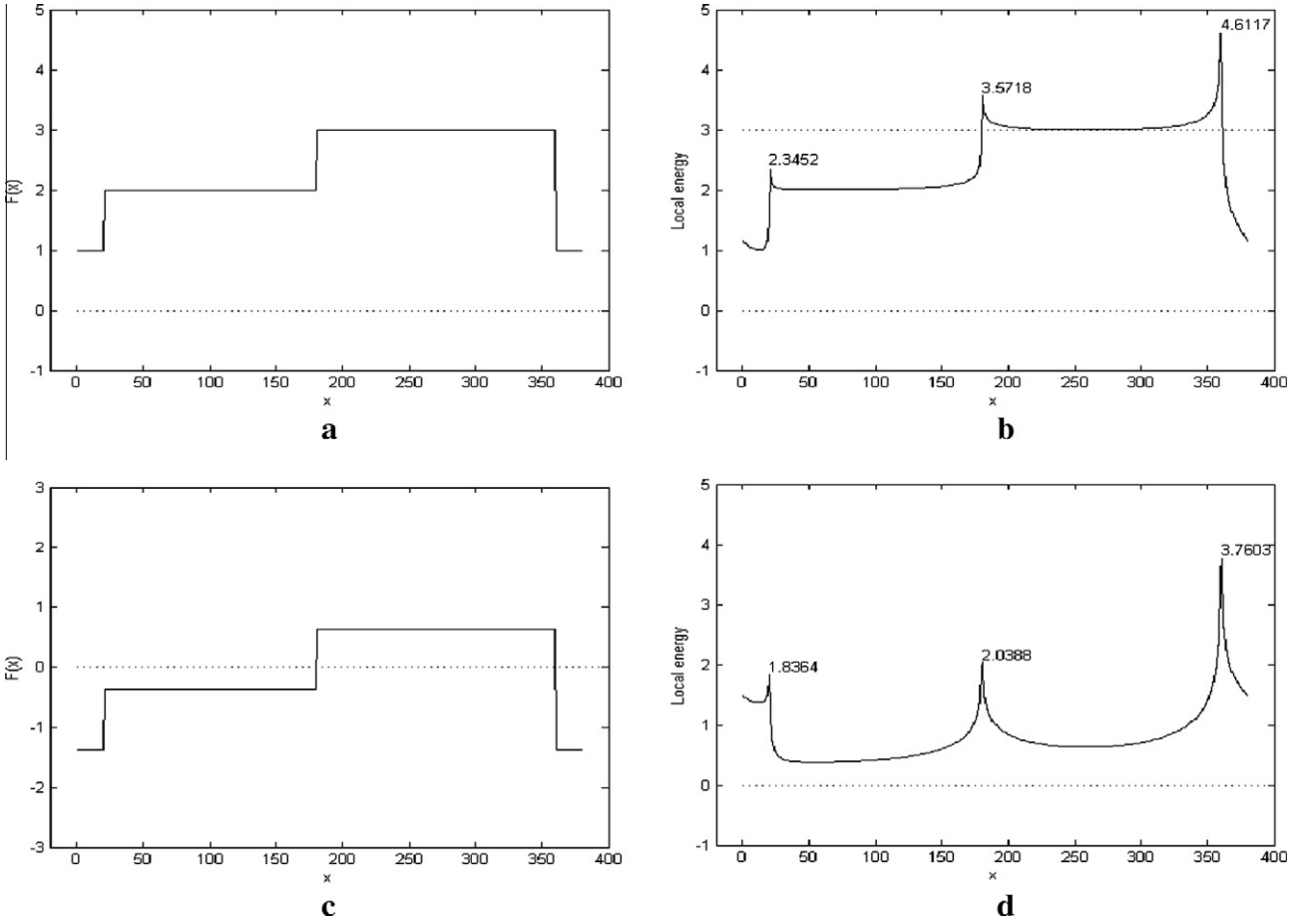

Fig. 4. The original signal (a) and the signal removed the DC component (c), and the corresponding local energy output (b) and (d).

Let $f(x,y)$ be the original image. Before calculating *PC* of image, there are three variants, $f_0(x,y)$ as $f(x,y)$ without the DC component, $\hat{f}(x,y)$ as the 2-D discrete Hilbert transform of $f(x,y)$, and the sum of Fourier amplitude $\sum_{m\times n} a_{m\times n}$, should be determined. Because *PC* calculated over the whole image is not accurate enough to locate features as shown in Fig. 4, we calculate *PC* by windowing the image. The following requirements are stipulated:

(1) A moving window is used to calculate *PC* at each point to keep the 1Hcontinuity of the image.
(2) As stated, DC component should be removed from the image.
(3) $f_0(x,y)$ and $\hat{f}(x,y)$ are calculated by convoluting image with two window functions.

We take the 1-D signal (Fig. 5a) as an example to understand the necessary of windowing. From Fig. 5b, we can see that it is difficult to distinguish features without windowing, even though *PC*s come to the considerable extreme value at feature points. While in Fig. 5c, *PC*s of feature points are close to 1 by windowing the signal, resulting in detecting features without difficulty.

It is too complicated to calculate *PC* of every point window by window. Thus, according to the function of 2-D discrete Hilbert transform (Eq. (14)) and the matrix of removing DC component (Eq. (19)), we make two operators *Mf* and *Mh* convolute the image to obtain $f_0(x,y)$ and $\hat{f}(x,y)$, respectively. The shape of operator *Mf* and *Mh* are illustrated in Fig. 6.

Using the operator *Mf* and *Mh*, the calculation of *PC* (Eq. (18)) can be expressed by

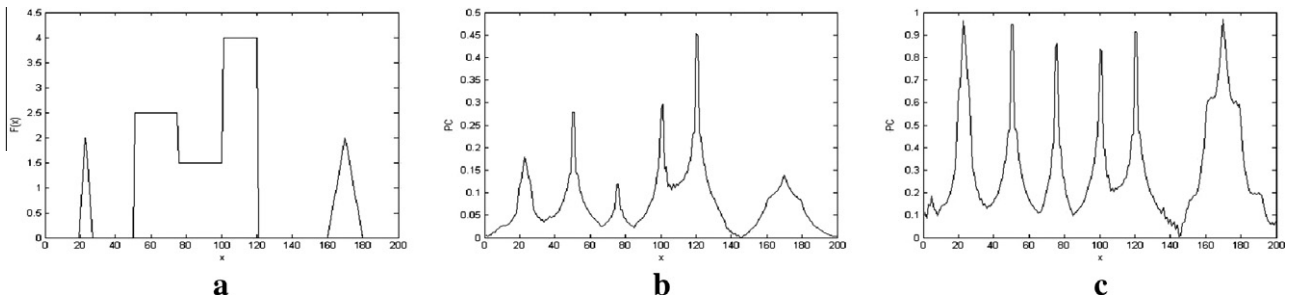

Fig. 5. The original signal (a), the phase congruency (b), and the phase congruency produced by windowing the signal (c). Note that the phase congruency in (c) is more outstanding at feature points.

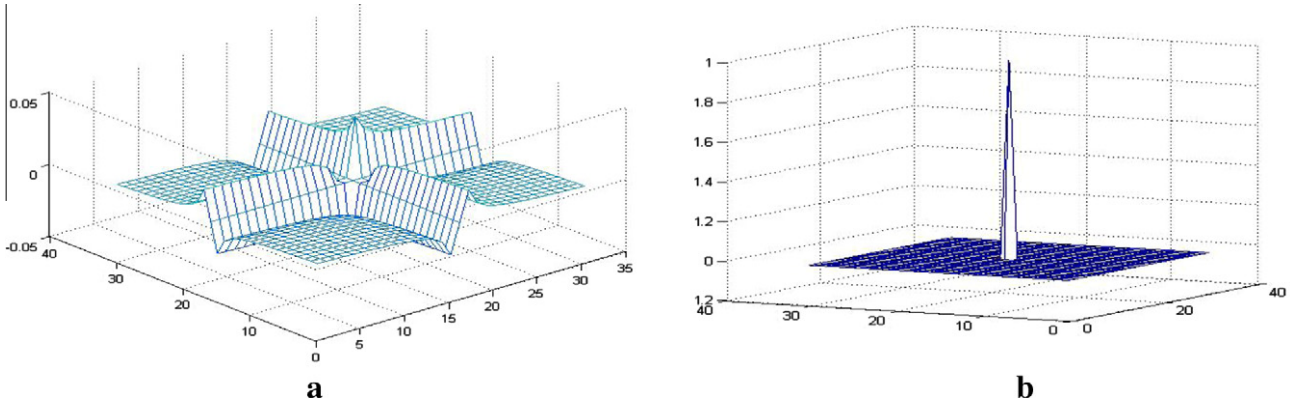

Fig. 6. The operator *Mh* (a) of 2-D Hilbert transform and *Mf* (b) used to remove the DC component from original image.

$$PC(x,y) = \frac{E(x,y)}{\frac{1}{MN}\sum_{u=0}^{M-1}\sum_{v=0}^{N-1}|F(u,v)|} = \frac{\sqrt{(Mf * f(x,y))^2 + (Mh * f(x,y))^2}}{\sum_{m\times n} a'_{m\times n}}, \quad (20)$$

where $M = m$; $N = n$; $f(x,y)$ is the original image; $a'_{m\times n}(\frac{1}{MN}|F(u,v)|)$ is the Fourier amplitude over the current window having been removed the DC component, namely the first harmonic component a_0.

Because the moving window shorts the image, some inconsequential image features, especially noise, will be extracted. A variable ε is added to the sum of Fourier amplitude to reduce noise and improve the quality of feature detection

$$PC(x,y) = \frac{E(x,y)}{\sum_{m\times n} a'_{m\times n} + \varepsilon}. \quad (21)$$

If ε is set as a constant, it is difficult to determine its value. Moreover, the size of window, the distribution of noise and the level of every pixel's illumination in window can affect the constant. Therefore, the variable ε should be connected with current window. Considering that DC component can reflect the level of illumination, we introduce the DC component as the variable ε to reduce the noise.

After adding the DC component to the sum of Fourier amplitude, the denominator of Eq. (21) can be expressed as the sum of Fourier amplitude over the current window without removing the DC component. So, the expression of *PC* is given by

$$PC(x,y) = \frac{E(x,y)}{a_0 + \sum_{m\times n} a'_{m\times n}} = \frac{E(x,y)}{\sum_{m\times n} a_{m\times n}}, \quad (22)$$

where $a_{m\times n}$ is the Fourier amplitude over the current window without removing the DC component.

From Eq. (21), *PC* of each point in the image arranges from 0 to 1. Since the DC component of original image has been introduced to reduce noise, *PC* of image features is not close but far below 1.0.

In summary, the implementation of calculation for *PC* requires the following steps:

(1) Input image $f(x,y)$ is convolved with the operator *Mf* and *Mh* to produce outputs $f_0(x,y)$ and $\hat{f}(x,y)$.
(2) Two outputs $f_0(x,y)$ and $\hat{f}(x,y)$ are squared and summed to obtain local energy.
(3) After extracting of square root, local energy is divided by the sum of Fourier amplitude $a_{m\times n}$ over the current window.

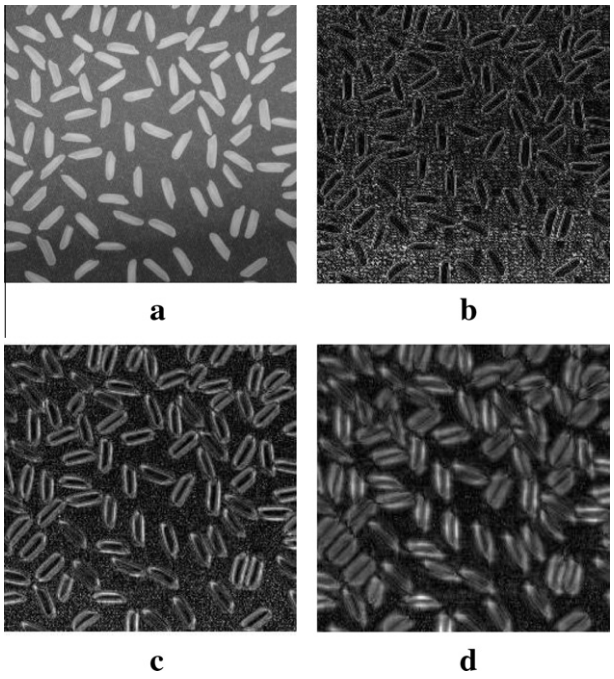

Fig. 7. (a) is original rice image, (b), (c) and (d) are the detection results using proposed phase congruency with the window size of 3, 5 and 7. Note that there is remarkable noise in (b), and features are more blurring in (d).

4. Result

In this section, some test images and the outputs from phase congruency based on 2-D Hilbert transform are presented. Fig. 7 shows three detection results of rice image using the proposed method with three different size of window. As shown in Fig. 7b, because the small size of window is chosen in the calculation, there is visible noise in the detection result. Fig. 7c illustrates an ideal output of detection. In Fig. 7d, the detection result from a larger size of window, we can see that the detection becomes more illegible. Thus, we should choose an appropriate size of window to calculate *PC* in order to reduce the noise, even though has added the DC component to the sum of Fourier amplitude.

Feature detection results of an image in BSDS are illustrated in Fig. 8 by using Canny operator, Sobel operator, wavelet algorithm, phase congruency model proposed by Kovesi and the proposed algorithm.

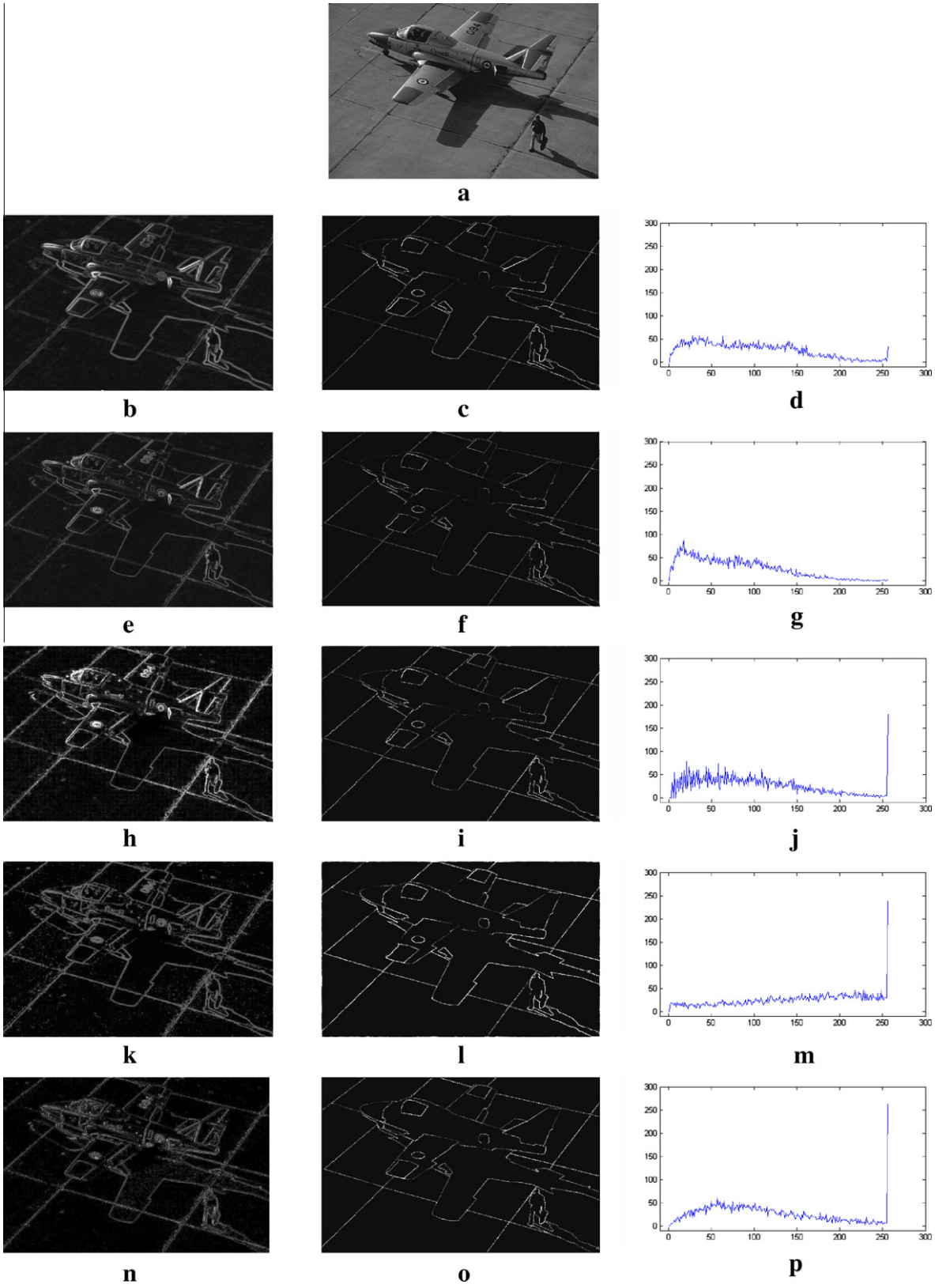

Fig. 8. Feature detection results of Fig. 6c by using Canny (b) and Sobel operator (e), Wavelet (h), Gabor (k) and the proposed algorithm (n), respectively. (c), (f), (i), (l) and (o) are the corresponding map with pixel kept based on edge map. (d), (g), (j), (m) and (p) are the number of the pixel distributing in the map at different gray level.

It is shown that detection results are influenced by the level of intensity gradient in the image markedly (Fig. 8b, e and h). In this paper, a systematical method is present to analyze the intensity distribution of detection results. We only keep the gray level of pixel from detection on edge map, and stretch the gray level to [0,255]. And then, the number of pixels distributing at different

gray level can be retrieved and shown in the left of Fig. 8. Fig. 8d and g show that the maximum number of pixel with high response is not at 255, and the response of most pixels scatter between 0 and 150. In Fig. 8j, the number of pixels at 255 is over 150, Even though Fig. 8j shows that the wavelet algorithm is influenced less from intensity gradient than Canny and Sobel method, some features detection with high response, like circle mark on the left wing, is not locate at the real edge. Further more, Fig. 8d, g and j evidently show that the level of response of detection results from the algorithm of Canny, Sobel and wavelet is not centralized, especially at the airplane nose empennage and circle mark on the left wing. As shown in Fig. 8m and p, the number of pixel at 255 is 239 and 263, respectively. Thus, by using the proposed algorithm, the detection result is closer at the highest response than other algorithm, and is influenced little by the intensity gradient of origin image.

Based on the formula of PC, there is an intimate relation between local energy of feature point and the sum of Fourier amplitude, thus, the response of detection result is more centralized and close to 1 (see Fig. 5c). As to the algorithm of Canny, Sobel and wavelet, the response of detection is influenced by the intensity gradient, so that the step edge has a stronger response of detection than ramp and roof. Consequently, using phase congruency method, the response of detection from as step, roof, delta and ramp is the same, even features with different level of intensity gradient.

Analytically, the speed of performance using the proposed algorithm is lower than Canny and Sobel operator. The detection using Canny operator and Sobel operator is implemented by convoluting the origin image with operator once, but it needs twice convolutions to retrieve the detection using the proposed algorithm. Thus, when the size of operator is the same, it takes more time to detect features using the proposed algorithm.

Table 1 compares computation time using Intel (R) Pentium(R) M-1.86 GHz processor with 512 Mo RAM running on Microsoft Windows XP for the Kovesi's algorithm and the proposed algorithm in his paper with Fig. 8a. Because parameters in both of algorithms have an influence on the speed of computation, we choose

Table 1
Comparison of the CPU times for detection between the Kovesi's algorithm and the proposed algorithm.

Technique	The Kovesi's algorithm	The proposed algorithm
CPU time (s)	10.016	6.156

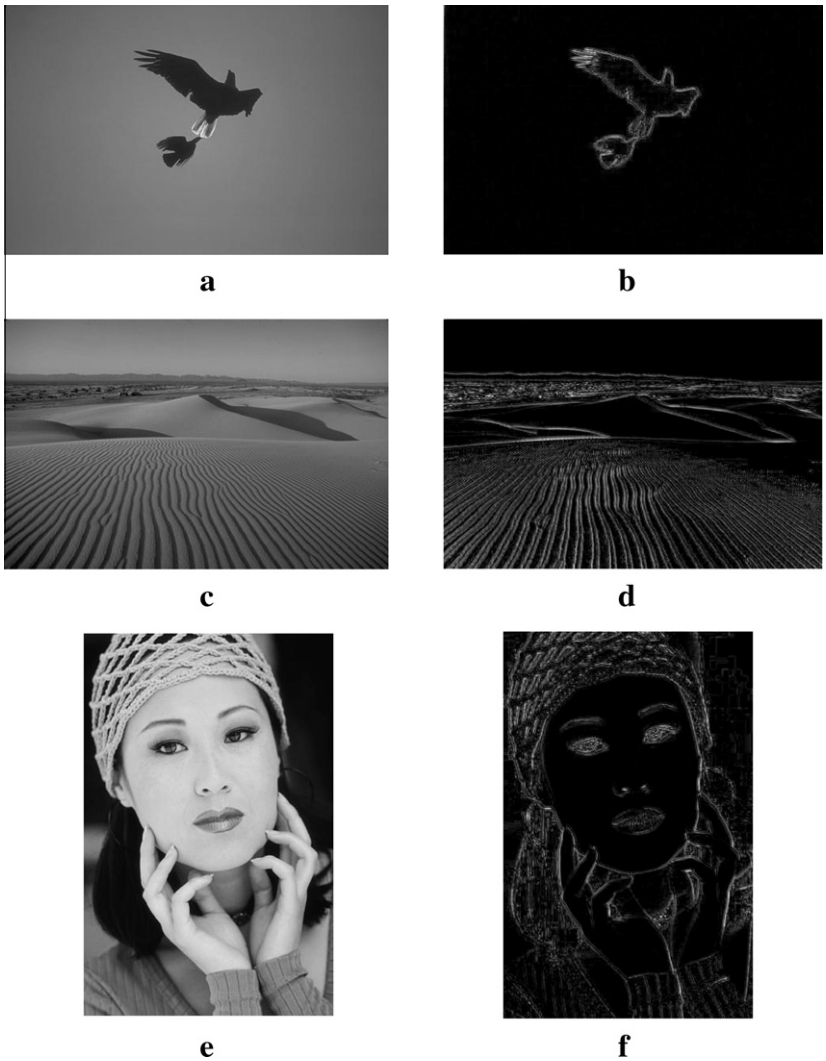

Fig. 9. Three test images from BSDS and feature detection results. (a), (c) and (e) are original images; and the corresponding feature detection from phase congruency shown in (b), (d) and (f).

optimal parameters for the good detection output. It takes 10.016 s to complete the detection (Fig. 8k) by using the Kovesi's algorithm with the number of filter scale and orientations being set 3 and 6, respectively. While the computation time of detection (Fig. 8n) by using the proposed algorithm with 5×5 window size, is only 6.156 s.

Fig. 9 illustrates feature detection outputs of three images in BSDS. In Fig. 9a, the two birds' color is darker comparing with the sky, except for the tail of the bigger one. The final detection (Fig. 9b) is distinct, not only at the dark edge but also at white edge. The texture of dissert, fringes of the shadow and the common boundary between dissert and sky in Fig. 9c, are illustrated clearly in Fig. 9d. Fig. 9f shows feature detection of an image of woman (Fig. 9e). Features from face, fingers, hair, and hat are retrieved distinctly.

Additionally, the proposed algorithm by this paper can also be applied into remotely sensed images (Fig. 10).

As shown in Fig. 10a, the image mainly includes factory buildings, roads and automobiles. Ground objects in Fig. 10b include farmland, pond, sideway and woodland. Remotely sensed image includes different ground objects and shadows, thus, it is more difficult to detect features than natural images. As shown in Fig. 11a, features like the boundary of factory buildings, shadows and automobiles, and the structure texture of road are detected commendably. And in Fig. 11b, detection results of the boundary of farmland, pond and woodland are also satisfied. The detection of Fig. 11a is better than Fig. 11b, because features are more regular in Fig. 11a. While, Features such as texture of woodland and farmland, the boundary of pond and sideway, are more complex, with the result that it raises the difficulty of feature detection in Fig. 11b.

According to test results, we obtain legible feature detections from natural image and remotely sensed image based on algorithm introduced in this paper. Additionally, as shown in Fig. 7, the scale of objects is similar. Thus, a suitable size of window can be chosen to retrieve ideal detection. While, the scale is not similar between features in Fig. 11, thus, feature detection results are imperfect.

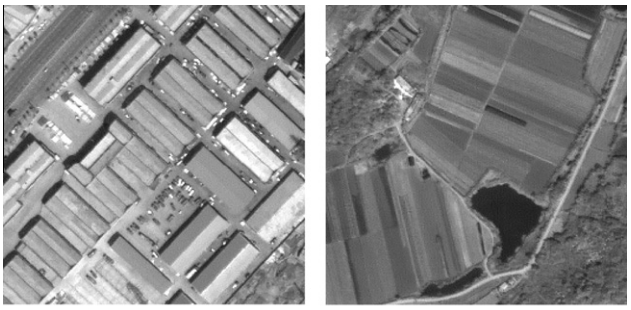

Fig. 10. Two test images from panchromatic band of IKONOS satellite covered Nanjing acquired on September 15, 2000.

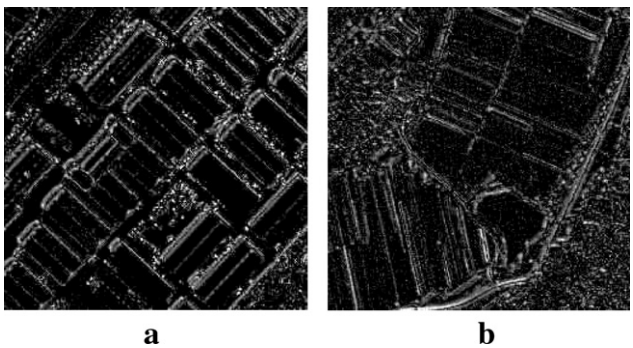

Fig. 11. The corresponding feature detection results of Fig. 9.

5. Conclusion

In summary, the method of phase congruency is implemented by computing the local energy defined by the 5Hquadratic sum of the value of the image and Hilbert transform, and then divided by the sum of Fourier amplitude. This traditional measure of phase congruency appears some difficulties to detect important features. The rectangular windowing function is introduced to the algorithm of phase congruency to detect all image features. However, the noise of image becomes more visible because of windowing.

Thus, we calculate local energy by using the 2-D Hilbert transform in all directions to avoid the inaccuracy of calculation of local energy with 1-D Hilbert transform. Meanwhile, the DC component of current window is introduced into the denominator of equation for calculating *PC* to reduce the influence of noise.

The proposed algorithm is compared with the existing feature detection algorithm in systematical way, and is tested by images in BSDS and remotely sensed images. The comparison and test results show that the proposed algorithm demonstrates considerable performance. It provides a new idea to detect image features based on the theory of phase congruency. There is still some deficiency of noise on the detection of image features, even though the algorithm of phase congruency has been modified to reduce noise. Therefore, further work is required to improve the algorithm and to control noise more efficiently.

References

Ahmed, Z., Sayadi, M., Faniech, F., 2009. Satellite images features extraction using phase congruency model. Internat. J. Comput. Sci. Network Security 9 (2), 192–197.

Bao, P., Zhang, L., Wu, X., 2005. Canny edge detection enhancement by scale multiplication. IEEE Trans. Pattern Anal. Machine Intell. 27, 1485–1490.

Bezalel, E., Efron, U., 2005. Efficient face recognition method using a combined phase congruency/Gabor filter bank technique. Proc. SPIE 5908, 437–444.

Bezdek, J., Chandrasekhar, R., Attikouzel, Y., 1998. A geometric approach to edge detection. IEEE Trans. Fuzzy Systems 6 (1), 52–75.

Blake, A., 1998. Active contours: The application of techniques from graphics, vision, control theory and statistics to visual tracking of shapes in motion. Springer, London.

Canny, J.F., 1986. A computational approach to edge detection. IEEE Trans. PAMI 8 (6), 679–698.

De Baets, B., Kerre, E., Gupta, M., 1994. The fundamentals of fuzzy mathematical morphology. Part 1: basic concepts. Internat. J. Gen. Systems 23, 155–171.

Demigny, D., 2002. On optimal linear filtering for edge detection. IEEE Trans. Image Process. 11, 728–1220.

Deriche, R., 1987. Using Canny's criteria to derive recursively implemented optimal edge detector. Intenat. J. Comput. Vision 1, 167–187.

Ducottet, C., Fournel, T., Barat, C., 2004. Scale-adaptive detection and local characterization of edges based on wavelet transform. Signal Process. 84 (11), 2115–2137.

Felsberg, M., Sommer, G., 2001. The monogenic signal. IEEE Trans. SP 49, 3136–3144.

Koplowitz, J., Greco, V., 1994. On the edge location error for local maximum and zero-crossing edge detectors. IEEE Trans. Pattern Anal. Machine Intell. 16 (12), 1207–1212.

Kovesi, P., 1999. Image features from phase congruency. Videre: J. Comput. Vision Res. 1 (3), 1–26.

Kovesi, P., 2000. Phase congruency: A low-level image invariant. Psychol. Res. 64 (2), 136–148.

Liu, Z., Laganiere, R., 2007. Phase congruence measurement for image similarity assessment. Pattern Recognition Lett. 28 (1), 166–172.

Lu, S., Wang, Z., Shen, J., 2003. Neuro-fuzzy synergism to the intelligent system for edge detection and enhancement. Pattern Recognition 36 (10), 2395–2409.

Mallat, S., Hwang, W.L., 1992. Singularity detection and processing with wavelets. IEEE Trans. Inform. Theory 38, 617–643.

Marr, D., Hildreth, E.C., 1980. Theory of edge detection. Proc. R. Soc. Lond. B, Biol. Sci. 207, 187–217.

Morrone, M.C., Burr, D.C., 1988. Feature detection in human vision: A phase-dependent energy model. Proc. R. Soc. Lond. B, Biol. Sci. 235 (1280), 221–245.

Morrone, M.C., Owens, R.A., 1987. Feature detection from local energy. Pattern Recognition Lett. 6 (5), 303–313.
Morrone, M.C., Ross, J.R., Burr, D.C., Owens, R.A., 1986. Mach bands are phase dependent. Nature 324 (6094), 250–253.
Osman, Z., 2011. Iris Recognition Using Phase Congruency. IICMS, pp. 341–344.
Perona, P., Malik, J., 1990. Detecting and localizing edges composed of steps, peaks and roofs. In: Proc. 3rd Internat. Conf. on Computer Vision, pp. 52–57.
Prewitt, J.M.S., 1970. Object enhancement and extraction. In: Lipkin, B.S., Roseenfeld, A. (Eds.), Picture Processing and Psychohistories. Academic Press, New York, pp. 75–149.
Punsawad, Y., Wongsawat, Y., 2009. Palmprint image enhancement using phase congruency. IEEE ROBIO, 1643–1646.
Read, R.R., Treitel, S., 1973. The stabilization of two-dimensional recursive filters via the discrete Hilbert transform. IEEE Trans. Geosci. Electron GE-11, 153–160.
Roberts, L.G., 1965. Machine perception of three dimensional solids. In: Tippet, J., Berkowitz, D., Clapp, L., Koester, C., Vanderburgh, A. (Eds.), Optical and Electro-optical Information Processing. MIT Press, Cambridge, pp. 59–197.
Sethian, J., 1996. Level-set Methods: Evolving Interfaces in Geometry, Fluid Mechanics, Computer Vision, and Material Sciences. Cambridge University Press, Cambridge.
Shen, J., Castan, S., 1986. An optimal linear operator for edge detection. In: Conf. CVPR'86, Miami, pp. 109–114.
Sobel, I., 1978. Neighborhood coding of binary images for fast contour following and general array binary processing. Comput. Graph. Image Process. 8, 127–135.
Struc, V., Pavesic, N., 2009. Phase congruency features for palm-print verification. IET Signal Process. 3 (4), 258–268.
Toivanen, P.J., Ansamaki, J., Parkkinen, J.P.S., Mielikainen, J., 2003. Edge detection in multispectral images using the self-organizing map. Pattern Recognition Lett. 24 (16), 2987–2994.
Xiao, P.F., Feng X.Z., Zhao S.H., 2006. Feature detection from IKONOS pan imagery based on phase congruency. In: Proc. SPIE, Image and Signal Processing for Remote Sensing XII, v6365.
Yi, S., Labate, D., Easley, D., Krim, H., 2009. A shearlet approach to edge analysis and detection. IEEE Trans. Image Process. 18 (5), 929–941.
Zetzsche, C., Barth, E., 1990. Fundamental limits of linear filters in the visual processing of two-dimensional signals. Vision Res. 30, 1111–1117.
Zhang, L., Bao, P., 2002. Edge detection by scale multiplication in wavelet domain. Pattern Recognition Lett. 23 (14), 1771–1784.
Zhang, L., Zhang, L., Mou, X., 2010. RFSIM: A feature based image quality assessment metric using riesz transforms. In: Internat. Conf. on Image Processing, pp. 321–324.
Zhang, L., Zhang, L., Mou, X., Zhang, D., 2011. FSIM: A feature similarity index for image quality assessment. IEEE Trans. Image Process. 20 (8), 2378–2386.